

Effects of Digital Elevation Model resolution on Rain-on-Grid simulations: a case study in a Slovenian watershed

Marcos Julien Alexopoulos^{1*}, Panayiotis Dimitriadis¹, Theano Iliopoulou¹, Nejc Bezak², Mira Kobold³ and Demetris Koutsoyiannis¹

1 Department of Water Resources and Environmental Engineering, School of Civil Engineering, National Technical University of Athens, 15780 Zographou, Greece; mjalexopoulos@gmail.com (MJA); tiliopoulou@hydro.ntua.gr (TI); dk@itia.ntua.gr (DK) 2 University of Ljubljana, Faculty of Civil and Geodetic Engineering, Jamova cesta 2, Ljubljana, Slovenia; Nejc.Bezak@fgg.uni-lj.si (NB)

3 Slovenian Environment Agency, Ljubljana, Slovenia; Mira.Kobold@gov.si (MK)

*Corresponding author: Marcos Julien Alexopoulos (mjalexopoulos@gmail.com)

ORC-IDs:

MJA: 0000-0002-7164-8547

TI: 0000-0001-7053-4348

PD: 0000-0003-4956-8820

NB: 0000-0003-2264-1901

MK:

DK: 0000-0002-6226-0241

Effects of DEM resolution on Rain-on-Grid simulations: a case study in a Slovenian watershed

The study evaluates the Rain on Grid (RoG) hydraulic model's sensitivity to Digital Elevation Model (DEM) resolution when simulating an extreme flood in Slovenia. The RoG model is validated against a high-resolution benchmark, showing strong agreement with a Kling-Gupta Efficiency of 0.913 and Pearson correlation of 0.964 for a 1 m DEM. Differences are observed in peak shapes and concentration times, attributed to rainfall propagation in RoG grids. DEM resolution significantly impacts performance, with the largest decrease between 1 m and 5 m resolutions. Coarser DEMs yielded higher depths, indicating slope decreases and terrain smoothing. The study concludes that high-resolution DEMs (<1m) are needed for adequate RoG performance, while commercially available coarser DEMs (30m) degraded accuracy and should be avoided using this method. Differences from semi-empirical concentration time models are also discussed, and an emphasis is given also on the impacts on water velocity and numerical stability.

Keywords: Rain on Grid, Validation against standard methods, DEM resolution resampling, Concentration time, Courant number, Slovenia

1. Introduction

Flood risk management and disaster risk reduction strategies necessitate accurate and advanced hydraulic modeling to reliably predict river flow and inundation patterns during various rainfall events (Huang et al., 2023, Su et al., 2022, Vázquez et al., 2023). Conventional rainfall-runoff models often encounter several limitations and semi-empirical assumptions, such as the use of hydrological methods in the literature for the construction of the runoff hydrograph (e.g., through the SCS method or the unit-hydrograph), the inability of simulating the runoff entering the river downstream of the runoff hydrograph's location, the use of semi-empirical expressions for the estimation of the concentration time that have been validated for watersheds of different geometric characteristics and climatic conditions. Similarly, the standard hydraulic modeling approaches are often requiring high computational demands, intricate complexity, and face challenges in capturing complex physical processes accurately (Guo et al., 2021, Sebastian et al., 2022).

The rain-on-grid (RoG) method presents a promising solution, aiming to improve the efficiency of both hydrological and hydraulic simulations (i.e., combining the hydrological rainfall-runoff model and the hydraulic flood-propagation).

To the authors' knowledge, there are few studies in literature exploiting this method. and validating it against standard rainfall-runoff. In addition, no study has accounted for the impact of the concentration time, the roughness parameter, and the Digital Elevation

Model (DEM) resolution on modeling results, which are considered as the most important sources of uncertainty compared to other model's input hydrological parameters and computational hydraulic parameters (Dimitriadis et al., 2016).

Al-Mamoon et al. conducted a study (Al-Mamoon et al., 2016) to compare the efficiency of the RoG method with the traditional approach of applying runoff hydrographs from hydrological models that correspond to sub-watersheds. The study was carried out in a Qatar watershed area that included the city of Doha, with the implementation of two sets of design rainfall - 10 and 100 years. The peak runoff rates generated by both methods were compared at five sub-watershed junctions. The study shows similar results amongst the two trials. However, there was only a slight difference of ± 0.05 m on average for flood extent between the RoG and traditional methods.

Costabile et al. (2021) assessed the potential of HEC-RAS 2D simulations (Costabile et al., 2021). The study evaluated the model's ability to reproduce simulations under different configurations that may lead to numerical instabilities. Specifically, the researchers used the RoG setup and conducted a trial on a small-scale watershed in Southern Italy. Their objective was to replicate a flood event that occurred between 27 and 28 January 2004. They indicate that the HEC-RAS 2D simulations using the RoG setup adequately reproduced the two-day flood event. However, the simulation overestimated the first peak but was able to better capture the two following peaks. Furthermore, the model failed to reproduce the recession limb of the total event hydrograph. The authors noted that these inconsistencies may be due to inappropriate model setup and lack of proper model calibration. Another study has observed success in utilizing the RoG technique within a source-pathway-receptor-consequence context to formulate a flood risk assessment over the Gospic watershed in Croatia (Krvavica et al., 2023). Additionally, RoG has demonstrated its efficacy in ascertaining hydrology and generating estimations for various loss-mechanisms such as roughness losses, infiltration losses, and depression storages for a given area (Coombes et al., 2018).

Zeiger and Hubbart (2021) conducted a study on the environmental flow targets of a sub-watershed in Central US, using an integrated approach of the Soil and Water Assessment Tool (SWAT) and the Hydrologic Engineering Center's River Analysis System (HEC-RAS) model (Zeiger & Hubbart, 2021). They aimed to quantify the event-based targets through generating the areal effective rainfall from SWAT and feeding it into the HEC-RAS simulation. The authors report varying run-times and stage hydrograph responses in the 2D HEC-RAS modeling while using different computational intervals. Uncalibrated simulations show unsatisfactory model performance; therefore, calibrating a RoG model is necessary.

Costabile et al. evaluated the impact of Digital Elevation Model (DEM) depression filling on the performance of 2D RoG modeling over four watersheds in Italy (Costabile et al., 2022). The study assumed spatially uniform and temporally constant rainfall and concluded that applying depression filling algorithms leads to faster computed discharges at the watershed outlet.

A study closer to the objectives outlined in the present research has been conducted by David and Schmalz (2021). This study focused on evaluating the interaction between spatial resolution (mesh and underlying DEM) and model parameter sensitivity. The study area was the Messbach watershed. In the first part, the model was run with varying mesh (1 m to 30 m) and DEM (0.25 m to 5 m) resolutions and compared to a high-resolution benchmark (1 m mesh, 0.25 m DEM) for validation of model performance. It was found that resolutions up to 5 m mesh and 1 m DEM gave comparable results. In the second part, further parameters like laminar depth, roughness, filters and precipitation data were evaluated. The study established that laminar depth and roughness were

sensitive parameters, while filter settings showed low sensitivity for the tested resolutions.

In the literature, studies have demonstrated the importance of DEM resolution in capturing hydrological processes. García-Alén et al., (2022) show the relevance of vertical accuracy over horizontal resolution of DEMs for modeling surface runoff. Finer vertical resolutions are necessary to accurately represent terrain features that influence hydrological responses. In contrast, the difference in horizontal resolution shows similar results in the outlet hydrograph. This contradicts the findings of Xu et al., (2021), who investigated the impact of various DEM resolutions and showed major differences in the flooded area, with greater areas inundated as the resolution coarsens. This finding is further supported by Muthusamy et al., (2021), who show that as the resolution of the DEM decreases (becomes coarser), there is a notable increase in both the flood extent and the mean flood depth. They attribute it to the reduced definition of the river channel at coarser resolutions, which leads to an underestimation of the river depth and, consequently, a reduction in channel conveyance. Furthermore, it has also been shown that the source of the elevation is also relevant according to the study region (Khojeh et al., 2022), while it may affect more inundation area rather the hydrograph response (Jing Li & Wong, 2010).

This study has multiple aims. Firstly, it seeks to validate the RoG hydraulic model in simulating an extreme 2007 flood in Slovenia that caused major damage. This event will be compared to a high-resolution benchmark from the Slovenian Environment Agency (ARSO) to assess the RoG method. Secondly, it quantifies the impact of DEM resolution on RoG simulation accuracy and performance. DEM characteristics are compared during the resampling process, and their integration to the model is also assessed. We do so by examining the impact on computation time, in addition to model outputs and numerical stability.

2. Materials and Methods

2.1. Study area

The Selška Sora watershed, situated in the northwestern part of Slovenia, spans an area of approximately 104 km² up to the gauging station Železniki. This landscape encompasses grasslands and agricultural lands, with a predominance of forested areas, which constitute around 84% of the total land use. The climate in this region is temperate, receiving an average annual precipitation of 1700 mm. The Selška Sora River drains the watershed and flows into the Sora River, which subsequently joins the Sava River. Its elevation is ranging approx. from 440 to 1600 m (Figure 1).

This region has witnessed a history of frequent flooding, with major flood events recorded in 1965, 1990, and 2010 (Komac & Zorn, 2013, Zorn & Komac, 2011). These floods have inflicted substantial damage to infrastructure and property. The geology is characterized by a complex interplay of sedimentary and meta-morphic rocks, exhibiting varying levels of permeability and hydraulic conductivity (Buser S, 2010).

One of the most significant flood events in the region occurred on September 18, 2007, (Rusjan et al., 2009). This Mesoscale Convective System (MCS) captured the attention of the scientific community and provided material for researchers to investigate various aspects of flood risk management. A selection of studies has been conducted to examine the factors that contributed to the severity of the flood event.

Rusjan et al. (2009) conducted a comprehensive evaluation of the storm event that occurred in western Slovenia and discovered that it resulted in some of the most severe rainfall rates ever recorded, surpassing the typical 100-year return period (Rusjan et al., 2009). This finding is consistent with the conclusions presented in the work of Zanon et al. (2010). Marchi et al. (2009) developed a methodology utilizing the flood event to emphasize the significance of post-flood surveys, especially in situations where flood discharge data is lacking (Marchi et al., 2009). Their approach involved utilizing the slope-conveyance and Manning Strickler methods to estimate the peak discharge. Additionally, they incorporated eyewitness accounts and crowd-sourced media materials to track the flood's progression and identify the time at which the discharge peaked.

2.2. Data and model set-up

To accurately simulate the flood event, an hourly rainfall time series was extracted for the period between 18/09/2007 00:00:00 and 19/09/2007 00:00:00 from ARSO weather station Davča. This station is an integral component of the gauge network maintained by ARSO and is located only 500 m from the watershed's centroid (Figure 1). Based on the findings of Rusjan et al., (2009) and Zanon et al., (2010), a uniform distribution is applied to the rainfall data over the modeling grid. To validate the performance of the hydraulic simulation, a time series for the Železniki station was extracted from the high-resolution benchmark run established in the study by Kobold (2007) using HEC-1 (Kobold et al., 2008; Kobold and Sušnik, 2001; WMS Manual: Watershed Modeling System. Reference manual, 1997). HEC-1 is a lumped hydrologic modeling software developed by the Hydrologic Engineering Center (HEC) to simulate rainfall-runoff processes. The program allows for event-based simulation using a variety of methods for computing loss, baseflow and flood routing components. HEC-1 was a widely applied hydrologic model before being succeeded by HEC-HMS. The benchmark simulation of the September 2007 event established by Kobold (2007) utilized watershed characteristics like area, slope, stream network properties, and land use. In addition, water marks extracted during the post-event survey by ARSO are used for areal comparison. Furthermore, using the final configuration, the model is modeled for another day on the 17/0/2010 where observations are available.

The RoG method in this study is implemented using the United States Army Corps of Engineers (USACE) HEC-RAS suite. HEC-RAS is an open-source software used for hydraulic calculations, that recently allowed the option to apply gauged or satellite rainfall directly as a boundary condition. 2D HEC-RAS allows the user to choose amongst the Diffusion Wave Equations (DWE), the original Shallow Water equations (SWE-ELM, which stands for Shallow Water Equations, Eulerian-Lagrangian Method); and a new Shallow Water equations solution that is more momentum conservative (SWE-EM, standing for Shallow Water Equations, Eulerian Method). In the present case study, the SWE-EM equations are solved utilizing a finite difference scheme. Predicated on the assumption that the horizontal length scale is significantly larger than the vertical length scale, the SWE are a set of hyperbolic partial differential equations, which provide a simplified but robust framework for describing flow dynamics.

The two-dimensional Shallow Water Equations employed in HEC-RAS 2D can be written as follows (Hariri et al., 2022). The continuity equation - encapsulating the principle of mass conservation:

$$\frac{\partial h}{\partial t} + \nabla(\mathbf{u}h) = R$$

And the momentum equation:

$$\frac{\partial \mathbf{u}}{\partial t} + (\mathbf{u}\nabla)\mathbf{u} + \frac{\nu_t}{h}(h\nabla\mathbf{u}) + g\nabla(h+z) = gS_f \quad 2$$

Where the unknowns are the water depth h and flow velocity vector u . The compound source R accounts for the terms of the water balance (e.g., precipitation, infiltration). The remaining parameters are defined as the acceleration of gravity g , the horizontal eddy viscosity coefficient ν_t , the bed elevation z , and the bottom friction coefficient S_f . By neglecting the viscosity and advection term, the diffusive wave approximation of the momentum equation can be rewritten as follows:

$$\frac{\partial \mathbf{u}}{\partial t} + g\nabla(h+z) = gS_f \quad 3$$

The equations are solved by setting boundary conditions on the watershed's domain. The DEM employed is derived from the high-resolution 1 m LiDAR ARSO dataset. Research investigating the vertical accuracy of DEMs has demonstrated that LiDAR datasets exhibit the lowest vertical error in comparison to other types of DEMs commonly utilized for hydraulic modeling purposes (Gonga-Saholiariliva et al., 2011). The United States Geological Survey (USGS) Curve Number (CN) method is utilized in this hydraulic setup to estimate the generation of runoff. For the land cover layer, the CN values are determined based on the CORINE 2006 land cover dataset, which features a spatial resolution of 100 m (Figure 2). An infiltration layer is calculated according to the CN layer. The typology, along with the corresponding CN and Manning values (landcover layer), and Abstraction Ratio (infiltration layer) are tabulated in Tables

Table 1. The Manning coefficients are selected based on local research practice. Furthermore, to capture the variations in permeability across the study site, we utilize the Copernicus Imperviousness data with a resolution of 20 m (Union, 2018). The selection of appropriate Manning's roughness coefficients (n values) for the different land cover types in the RoG model involved an iterative process of testing different values guided by standard ranges from literature and adjustment based on site-specific conditions. Initial n values were assigned based on common tabulated values for overland flow on similar land cover categories (Chow, 1959, Engman, 1983).

An orthogonal mesh with a resolution of 50×50 m was implemented to cover the entire study area. However, to better capture the topographic relief and improve the accuracy of the hydraulic simulation, refinement regions were formed across the main channel. The refinement regions were designed with a higher resolution than the original Cartesian mesh, ranging between 4 and 10 m for the near spacing and between 1 and 3 for the near repeats, depending on the topographic relief. The selection of the resolution of the refined regions is based on the findings of David and Schmalz (2021). The far spacing was set at 50 m to match the original Cartesian mesh. The refinement regions were implemented to increase the grid resolution in areas of higher hydraulic complexity, such as the main channel, and to better represent the hydraulic processes occurring in these regions.

2.3 Courant number

The Courant number provides a condition for convergence while solving certain partial differential equations numerically using explicit time integration schemes. It can be

interpreted as the ratio of the physical time step size to the maximum allowable time step size for numerical stability. It is defined as:

$$C_r = \frac{u\Delta t}{\Delta s} \quad 4$$

Where u is the wave propagation speed, Δt is the time step size, and Δs is the spatial discretization step size. For numerical stability, C_r must be less than or equal to 1 for explicit schemes, but in implicit schemes larger values (e.g., 3 for the full Saint-Venant momentum equation to 5 for the diffusion-wave method) may be allowed but not generally recommended, since this condition ensures that the numerical domain of dependence contains the physical domain of dependence. When $C_r > 1$, the numerical method becomes unstable as information can propagate further in a single time step than the spatial discretization allows. In the current configuration, after several trials the RoG model became stable by defining the Courant number between $C_{\min} = 0.45$ and $C_{\max} = 1.0$, with a computational interval of 1 min, which may result in the maximum range below for the timestep Δt :

$$\frac{\Delta x_{\min} C_{\min}}{u_{\max}} \leq \Delta t \leq \frac{\Delta x_{\max} C_{\max}}{u_{\min}} \quad 5$$

where Δx_{\min} and Δx_{\max} , and u_{\min} and u_{\max} , are the minimum and maximum values for the spatial resolution of the computational grid and for the velocity, respectively. This means that the product of the velocity and the timestep can reach values between $0.45 \leq u\Delta t \leq 50$, and therefore, for the minimum fixed timestep of HEC-RAS (i.e., $\Delta t_{\min} = 0.1$ s), the maximum velocity at the smallest grid resolution (i.e., $\Delta x_{\min} = 1$ m) could be $u_{\max}(\Delta x_{\min}) = 5.5$ m/s.

The numerical configuration of the model is illustrated in Table 2.

2.4 Time of concentration

The time of concentration (T_c) represents the longest time required for water to travel from the furthest point in a watershed to a specified outlet. It is a valuable tool to predict the temporal distribution of runoff at the outlet of a watershed area. A variety of empirical and semi-empirical formulas have been developed over time. In this study, the T_c derived from the RoG simulation is compared against the time of concentration calculated using the Giandotti and Kirpich formulas. The Giandotti formula, commonly used across many European countries, is given by:

$$T_c = \frac{4\sqrt{A} + 1.5L}{0.8\sqrt{H}} \quad 6$$

Meanwhile, the Kirpich formula, often used for small rural watersheds, is given by:

$$T_c = 0.0078 \cdot L^{0.77} \cdot S^{-0.385} \quad 7$$

Where T_c is the time of concentration (Giandotti (h), Kirpich (min)), A is the watershed area (km^2), L is the length of the water channel (Giandotti (km), Kirpich (ft)), H is the difference in between outlet and mean watershed elevation (m) (for the Giandotti formula), and S is the mean watershed slope (for the Kirpich formula). It is important, however, to note some limitations in the use of these formulas. The Giandotti principle was formulated from watersheds with an area spanning at least 170 km^2 , making it potentially less accurate for the present watershed (104 km^2) while the Kirpich formula ignores important watershed characteristics such as area, surface roughness or land use, and assumes a uniform slope.

3. Results

3.1. RoG performance

Table 3 presents the KGE (Kling-Gupta Efficiency) (Gupta et al., 2009), Pearson correlation coefficient, and RMSE (Root Mean Square Error) of RoG simulation compared to the ARSO high-resolution benchmark run. The RoG simulation achieved a KGE value of 0.913, indicating a good level of agreement. The Pearson correlation coefficient of 0.964 suggests a strong linear relationship between the RoG simulation and the ARSO benchmark. The RMSE value of 22 indicates a significant difference between the simulated values and the benchmark observations.

Figure 3 displays the simulation results in the Železniki station. It is evident that the initial peak in the RoG hydrograph is significantly sharper.

Table 4 displays the time of concentration for the first and second peak derived from the RoG simulation, in addition to the time of concentration calculated from the Giandotti and Kirpich formulas.

Figure 4 shows the maximum water depth in the Železniki station, with depths ranging between 8-11 m. Figure 5 provides a close-up of the main reach.

Figure 6 presents the time series for the validation simulation for 17/09/2010. The simulation fits well observations, however there is a slight delay in the peak of the discharge by approximately 2 h. The RMSE score for this discharge simulation is $2.70 \text{ m}^3\text{s}^{-1}$.

3.2. DEM characteristics

Figure 7 provides an analysis of the main DEM statistics. As the resolution coarsens, fluctuations are observed in the minima, mean and maxima. Table 5 presents the coefficient of variation (CV) for different resolutions, ranging from 1 m to 30 m. The CV values remain remarkably consistent across all resolutions, hovering around 29.6%. The plots of mean, maximum slope and standard deviation of slope against DEM resolution all show a decreasing trend (Figure 8).

Figure 9 displays the relative frequency distribution of elevation for the 1 m and 30 m resolution DEMs.

3.3. Effect of DEM resolution in hydraulic output

Table 6 presents the comparison of KGE values, Pearson correlation coefficients, and RMSE values for different DEM resolutions, ranging from 1 m to 30 m.

Figure 10 displays the scatterplot relating the same RMSE and KGE values against the resolution, while Figure 11 illustrates the time series of the benchmark run against the RoG ensemble.

The impact of resolution on peak discharge values can be elucidated through

Table 7, which showcases the peak discharge values for the first and second peak.

Furthermore, to assess the impact of coarser DEM resolutions on the depth estimation, the depth rasters corresponding to each run were subtracted from the original depth raster generated using the 1 m DEM. Therefore, six different rasters are produced, each representing the absolute difference of water depths between a base resolution of 1 m and the remaining DEMs. Figure 12 illustrates the box plot corresponding to each depth-difference raster. Figure 13 displays the computation times for each resolution.

Figure 14 (a) displays the rating curves for the 1 m and 30 m DEM and Figure 14 (b) shows corresponding volume accumulations at the Železniki station over time.

Figure 15 illustrates the Courant number derived from the RoG simulation at the 12:15 PM timestamp, using the 1 m and 30 m DEM. For the sake of clarity, only the area towards the outlet is shown, as for the entire watershed differences are not visible.

Table 8 offers a comparative analysis of the Courant numbers across 1 m and 30 m DEM resolutions.

Figure 16 presents the maximum velocity near the outlet, identical to the area depicted in Figure 15. As anticipated, the 30 m DEM shows a larger inundated area.

4. Discussion

4.1 Impact of DEM Resolution on RoG Model Performance

An important contribution of this study is that it provides an exhaustive list of results for different dem resolutions for the relatively novel RoG method. While previous research has examined the effects of DEM resolution for traditional hydrodynamic and hydrological models (Podhorányi et al., 2013, Saksena & Merwade, 2015, Vozinaki et al., 2016), we felt a more thorough study on the matter would be beneficial to the current literature.

In this study, the performance of a RoG model on reproducing a flood event has been assessed, and the impact of roughness, CN, and DEM resampling has been evaluated on the hydraulic output, with more focus on the latter factor. The simulated values show good agreement with the ARSO high-resolution benchmark run (acquired with the typical hydrological rainfall-runoff methods). However, there are significant differences

observed in the peak shapes, specifically the initial peak, in the RoG hydrograph. In Figure 3, the maximum intensity of the rainfall event is observed at 12:15, and the second at 17:15. The use of an independent (to the surrounding land-use) value for the channel's roughness was found to improve the model's performance, which was set at 0.19 based on the post-calibration process and the Chow (1959) classification by creating a new land-use zone around the channel's width. Nevertheless, modifying the channel's roughness (around the 0.19 value) did not significantly affect the timing or speed of the simulated hydrographs, contrasting the findings of Ryan et al. (2022). Rather, increasing the Manning's n value served to attenuate the first and second peak discharges of the hydrographs. This discrepancy may be due to the unique propagation of rainfall within the 2D mesh of the RoG grid cells, which considers the total area that receives precipitation at each time step.

It has also been shown that both simulations display a shorter time of concentration in comparison to concentration times derived by means of empirical formulae. The Giandotti formula is closer to the time derived from the RoG simulation (1 hour and 45 min) than the Kirpich formula, which estimates a time of concentration of 6 hours and 48 min. The Muskingum-Cunge method for flood routing leads to a longer time to peak.

Furthermore, the RoG hydrograph exhibits a second peak approximately $20 \text{ m}^3\text{s}^{-1}$ higher than the ARSO hydrograph during the simulation. During the occurrence of the second peak, the soil had already reached its retention capacity, resulting in a higher volume of runoff water and consequently causing a higher second peak in the hydrograph.

In Figure 4, the flood extent represents the maximum water depth that occurred during the simulation of the flood event at any given point within the study area. This means that the snapshot provided does not present a realistic view of the flood propagation over time. Instead, it provides a snapshot of the maximum water depth that occurred at any specific location during the modeled flood event. In the area adjacent to the watershed outlet, the overestimation of the flood extent does not imply an excessive amount of water flowing through the main channel.

Analyzing the contour lines derived from the DEM with a 5 m interval (Figure 5), the areas where the RoG method overestimates water are at higher elevations ($>450 \text{ m}$) compared to the main inundation area (445 m and below). This implies the overestimation primarily occurs in elevated regions located outside the main channel. The overestimated flood extent observed in Figure 4 and Figure 5 can be attributed to the water quantity propagated from the two tributaries located north of the outlet during the simulation.

As expected, our results demonstrate that DEM resolution affects the performance of the RoG model in simulating flood events. Finer resolutions (1 m) capture the important topographic details that enhance the representation of drainage. This is somewhat consistent with the findings of Habtezion et al., (2016). Our study shows that coarser DEM resolutions tend also to underestimate discharge peaks compared to finer resolutions. However, our threshold varies, and a significant difference is visible past the 5 m resample. This applies also to the performance scores. In addition, our results support their finding that the mean slope declines as pixel size is increasing in a similar fashion.

4.2 DEM Resolution Effects on Flood Characteristics

When resampling, small fluctuations in various statistics such as the minima and maxima, as well as the mean, standard deviation, and coefficient of variation) are observed, and large differences occur in the water depths and flood volume. These fluctuations (rather than systematic trends) occur due to the changing spatial representation and averaging

effects introduced by the larger grid cells. When transitioning from a 1 m to a 5 m resolution, nearby high elevation points are blended, resulting in an increased maximum value. The mean and minimum values may also consistently increase due to the incorporation of larger-scale topographic features that were previously not fully captured in the finer resolution. Likewise, for the transition from 15 to 20 m resolution (minima), the change in grid cell size introduces a larger area being averaged together. Additionally, the standard deviation exhibits a noticeable trend. Coarser resolutions tend to have slightly higher standard deviations, suggesting increased variability in the elevation values within the larger grid cells.

As the resolution becomes coarser (Figure 8), the averaging that occurs results in lower mean slopes, maximum slopes and standard deviations. As grid cells get larger in coarser resolutions, smaller gradient slopes are lost and averaged out, resulting in the observed decreases. In contrast, the plot of minimum slope is relatively stable across DEM resolutions. This consistency indicates that the gentle slopes which dominate the landscape are still captured.

It is expected that the count of observations would decrease as the resolution is coarsened, due to the reduction in pixel count in the coarser DEM. The introduction of additional values in the 450 and 500 elevation bins when coarsening to a commercial resolution is consistent with the smoothing and averaging process. This can result in the blending of nearby elevation values, leading to a broader range of values being represented within the lower-range bins. Furthermore, the observation that the bin range towards the maximum values (bins 1600, 1650, and 1700) becomes more prominent in the coarser resolution aligns with the findings from Figure 7. The increased prevalence of values in the 1000-1200 m elevation range and 1300-1350 m elevation range in the 1 m raster, also suggests the presence of smaller-scale features. Instead, the 30 m resolution exhibits a bias towards higher dominance in the 700-1000 m elevation range, which corresponds to larger-scale topographic features.

For all the evaluated metrics (Table 6), the most significant decrease occurs between the 1 m and 5 m resolutions. The Pearson correlation coefficient remains relatively stable and consistently high, exceeding 0.9 for all resolutions. In terms of RMSE, the results demonstrate that transitioning from 1 m to 5 m resolution leads to an immediate increase in estimation errors of approximately $10 \text{ m}^3 \text{ s}^{-1}$. Beyond this point, the model performance remains relatively similar for 5 m and 10 m resolutions but starts to deteriorate as the resolution becomes coarser. The 25 m resolution exhibits poorer performance compared to the 30 m resolution and other selected resolutions. The 25 m resolution is shown to underestimate the most (Figure 11).

The KGE performance is reaching around 90%, with the 1 m resolution. As the resolution coarsens, the KGE values decrease. The 20 m resolution performs slightly better than the 15 m resolution, which contrasts with the RMSE scores. This difference may be attributed to the squared ratios of average and standard deviation values within the specific metric. It is evident that regardless of the metric used, approximately 70% of the variation in model performance can be attributed to the resolution. However, more data may be needed to achieve statistical significance. Overall, the performance metrics show that DEM resolution is significantly affecting modeling performance in a 2D domain, whereas it is not the case in e.g., 1D modeling (Md Ali et al., 2015).

In Figure 11, the initial peak of the hydrograph demonstrates an increased abruptness and delayed occurrence as the DEM resolution becomes coarser. Specifically, the rising limb initiates at approximately 10:30 AM for the 1 m DEM resolution, while for the 5 m and 10 m resolutions, the initiation time is delayed to 11:15 AM. Subsequently, for resolutions

ranging from 15 m to 30 m, the first peak appears at 11:45 AM. Coarsening the resolution results in a decrease in the magnitude of both the first peak and subsequent peaks, which agrees with the findings of Clark et al., (2015). Additionally, the lag time exhibits fluctuations between 13:30 and 13:15, although the differences are not significant.

It demonstrates a decreasing trend in the first peak discharge values as the resolution becomes coarser, with the 30 m resolution accounting for a loss of approximately 30 m³ at the time of peak. The second peak discharge values demonstrate a fluctuation in response to coarser resolutions.

At a first glance, it is evident from the box plots that the median values for all comparisons are negative, suggesting that coarser resolutions generally yield higher water depths (Figure 12). This agrees with the findings of Saksena and Merwade (2015) and Xafoulis et al. (2023), whose work shows that coarser resolutions lead to larger depths (Saksena & Merwade, 2015, Xafoulis et al., 2023). This trend is also reflected in the lower quartiles, which are predominantly negative across all resolutions. The effect of larger depths may be also attributed to the decrease of the average slope as resampling iterations are performed (Figure 8). Additionally, the box plot corresponding to the 5 m difference raster displays a notably larger interquartile range and whisker range compared to those for the remaining coarser resolutions.

Figure 13 reveals a significant difference in computation time when resampling the 1 m to the 5 m resolution, with a reduction of approximately 6 min. Interestingly, this drop in computation time is not consistent as the spatial resolution is further coarsened. This aligns with the findings from Figure 8, where the sharpest drop in standard deviation of the elevation slope occurs between these two resolutions. Also, the results show that the numerical solution of the model is not significantly impacted when the resolution of the DEM is resampled to resolutions coarser than 5 meters. Furthermore, the points derived from Figure 13 lead to the following power equation:

$$y = 16.285x^{-0.142} \quad 8$$

Where y the computation time (min) and x the DEM resolution (m). The DEM resolution accounts for 87% (R²) of the data variation in the computation time. The power function resembles the findings of David and Schmalz (2021):

$$y = 17.103x^{-3.308} \quad 9$$

Equation 9 is derived from a selection of finer DEM resolutions corresponding to 0.25, 0.5, 1, 2, 3, 4, and 5 m, with an R² of 99%. The exponents differ, with the David & Schmalz equation having a larger magnitude exponent. This results in their curve decreasing more rapidly with coarser DEM resolution. Regarding the rating curves (Figure 14): with the 1 m resolution, we observe a steeper rise in water levels with increasing discharge. This steepness is indicative of a river cross-section with a narrower and deeper channel. Conversely, the 30 m resolution rating curve is more gradual, indicating a wider, shallower river channel.

There are discrepancies in the model propagation between the two simulations (Figure 15): calculations are absent in specific regions like the area upstream of the channel and the two tributaries merging at the outlet when using the 30 m DEM. This can be attributed to the differences in connectivity, leading to a more extensive inundation in the selected timestamp within the modeling domain. In terms of the Courant number, the general range is between 0 and 0.4 across the extent, while it fluctuates between 0.6 and 1.0 within the main channel. However, certain regions violate the Courant criterion for both DEMs,

particularly upstream regions and areas where water converges towards the outlet. There is a greater number of regions with numerical instability in the 30 m DEM, particularly within the channel. It needs to be mentioned that numerical instability issues could be resolved by reducing the computational step and adjusting the maximum number of halving base time step accordingly, however these modifications were not implemented in the current runs, to understand how the DEM resolution is affecting the numerical solution.

In Table 8, the 1 m DEM resolution has a lower minimum and mean Courant number at 10-7 and 0.22 respectively, which is implying a broader range and fewer average violations of the Courant criterion compared to the 30 m DEM resolution. On the other hand, the 30 m DEM resolution, with a maximum Courant number of 7.63 and a mean of 0.36, shows more severe and frequent Courant criterion violations, which is consistent with the snippet illustrated in Figure 15. The maximum Courant number is reaching values of up to 2 in the area specified, however values are exceeding it in other parts of the domain. The standard deviations, 0.47 for 1 m and 0.50 for 30 m, suggest a similar distribution.

When it comes to velocities, the finer 1 m DEM resolution exhibited a broader velocity range and higher average velocities compared to the coarser 30 m DEM resolution. While the velocity distribution does not significantly differ between the two DEMs (Figure 16), the 30 m DEM shows a tendency to estimate lower velocities ($0-3 \text{ ms}^{-1}$) than the 1 m DEM. Despite this, areas characterized by velocities of $0-3 \text{ ms}^{-1}$ and $3-6 \text{ ms}^{-1}$ remain consistent across both resolutions. In Table 9, the mean velocity is higher for the 1 m DEM resolution (1.53 ms^{-1}) than for the 30 m DEM resolution (1.38 ms^{-1}). The maximum velocity recorded is notably higher for the 1 m DEM resolution (15.28 ms^{-1}) than the 30 m DEM resolution (10.19 ms^{-1}), indicating more extreme velocity peaks in the finer resolution. The standard deviations are similar for both the 1 m and 30 m resolutions. Compared to the analysis for the Courant numbers (Figure 15, Table 8), hereby the velocity range (ms^{-1}) map depicted in Figure 16 is adjusted according to the entire raster area, not the area depicted on the map like Figure 15.

In the context of landscape analysis, our findings are consistent with those of Bernard et al., (2022). We also observed that inundation area increases, and flow velocity rates decrease significantly as DEM resolution becomes coarser. Bernard et al., (2022) demonstrated that for a channel cross-sectional area of 105 m^2 , the mean flow width varies from 2 m to 14 m as pixel size increases from 1 m to 10 m. This resampling to coarser resolutions hinders the ability to properly represent channel geometry and floodplain inundation. Similarly, in our study area with a maximum channel width of 15 m, we found that a DEM resolution past 25 m (where we notice sudden difference in discharge peaks) was too coarse to fully capture the detailed channel morphology. On that note, perhaps it could be used as a benchmark threshold for landscape analysis. For example, in frameworks focusing on understanding how heterogeneous a drainage landscape is, e.g., Costabile et al., (2024). Resampling introduces increased and sometimes artificial connectivity between drainage cells, and we show that past the 5 m mark it would not be sound to use such a resolution for classifying ephemeral tributaries, or other elements of the landscape that contribute to the drainage process.

4.3 Limitations and Future Work

Several limitations make up part of this study. Specifically, the CN method is accounting for soil infiltration properties in our study, amongst the other options made available in

the HEC-RAS suite. On small temporal scales, the CN method tends to show comparable results to the Green-Ampt method (Ficklin & Zhang, 2013). It must be emphasized, however, that the CN method represents an empirical methodology, which, while widely accepted and applied in practice, carries a set of assumptions that may not hold true in the present scenario. Several studies have postulated that to attain an accurate representation of runoff, hybrid approaches are more suitable (Baiamonte, 2019, Jun Li et al., 2015, Viji et al., 2015). A spatial distribution of errors analysis would have been beneficial in identifying specific locations where the model performs poorly or exceptionally well. This could provide a more granular understanding of the model's performance and perhaps give insights into how different properties across the modeling domain might influence the results. However, with the amount of validation data available it was not feasible.

Another limitation of the present study pertains to the extent of the carried sensitivity analysis. Although we evaluated how the model responds to varying DEM resolution, a more comprehensive sensitivity analysis would offer a broader understanding of the model's performance under varying conditions, and would assess the model's response to alterations in key parameters such as geometry characteristics, soil infiltration methods, Curve Number values, Manning's coefficient values, as each of these variables can significantly influence the model output and in what hierarchy and degree (Dimitriadis et al., 2016).

Regarding the water depths calculated in our study, it is important to acknowledge that the temporal resolution of the rainfall input in the RoG simulation is also relevant. Previous research has shown that higher temporal resolutions lead to higher simulated water depths and changes in hydrograph shapes. Using sub-hourly rainfall data as input to RoG models results in earlier arrival times of the flood wave compared to coarser temporal resolutions. On the same token, it is also worth noting that our results may vary based on the type of rainfall event. For higher return periods, we would expect different arrival times of the flood wave at the outlet. Due to loss parameters, more improbable events such as return period of T100 vs T10 would yield a difference in the shape of the hydrograph. We would expect a sharper peak as the probability of the event is lowered, and based on our findings, we would expect that DEM variability for rainfall events of lower magnitude would be less evident. Since coarsening the DEM increases connectivity and channel width, we would expect much greater differences in modeled velocities and depths, as for lower magnitude events the velocities would decrease even more sharply as the DEM resolution coarsens in the main channel. For small tributaries, velocities would increase as more connectivity is introduced across the modeled domain. However, that would be an additional point of interest for future study.

5. Conclusions

Our study has provided insights into the application of RoG and its sensitivity to DEM resolution, which will benefit researchers and practitioners in the field of hydrology. The main findings can be summarized as follows:

- The RoG model shows good agreement with the high-resolution benchmark run, but there are differences in peak shapes and timing of the hydrograph.

- DEM resolution significantly affects the performance of the RoG model in simulating flood events, with finer resolutions (1 m) capturing important topographic details that enhance drainage representation.
- Coarser DEM resolutions tend to underestimate discharge peaks and exhibit delayed and more abrupt initial peaks compared to finer resolutions.
- Coarser resolutions generally yield higher water depths and lower flow velocities due to decreased average slopes and increased connectivity between drainage cells.
- The most significant decrease in performance metrics occurs between 1 m and 5 m resolutions, with approximately 70% of the variation in model performance attributable to resolution.
- Computation time decreases significantly when resampling from 1 m to 5 m resolution, but the reduction is not consistent with further coarsening.
- The numerical solution of the model is not significantly impacted when the DEM resolution is resampled to resolutions coarser than 5 meters.
- A DEM resolution past 25 m may be too coarse to fully capture detailed channel morphology and floodplain inundation in small watersheds.

Authors' contribution

Conceptualization: MJA, TI, PD, DK; Methodology: MJA, TI, PD, DK; Software: MJA; Validation: MJA, TI, PD, NB, DK; Formal Analysis: MJA, TI, PD, NB, DK; Investigation: MJA, TI, PD; Resources: NB; Data Curation: MJA; Writing—Original Draft Preparation: MJA; Writing—Review and Editing: TI, PD, NB, DK; Visualization: MJA, TI, PD, NB, DK; Supervision: TI, PD, NB; Project Administration: DK; All authors have read and agreed to the published version of the manuscript.

Acknowledgements

The authors would like to thank the anonymous reviewer and the editor for their constructive feedback, which assisted in the development of the final version of the manuscript.

Disclosure statement

The authors declare no conflict of interest.

Data availability statement

Data available on request from the corresponding author

Funding

This research received no external funding.

References

- Al-Mamoon, A., Regan, B., Sylianteng, C., Rahman, A. & Qassem, H. (2016)
Comparison of two modelling approaches for a pilot catchment flood study in
Qatar. *37th Hydrology and Water Resources Symposium 2016: Water,
Infrastructure and the Environment, HWRS 2016* 2016-Novem(November).
- Baiamonte, G. (2019) SCS Curve Number and Green-Ampt Infiltration Models. *J
Hydrol Eng* **24**(10). American Society of Civil Engineers (ASCE).
doi:10.1061/(ASCE)HE.1943-5584.0001838
- Bernard, T. G., Davy, P. & Lague, D. (2022) Hydro-Geomorphic Metrics for High
Resolution Fluvial Landscape Analysis. *J Geophys Res Earth Surf* **127**(3). John
Wiley and Sons Inc. doi:10.1029/2021JF006535
- Buser S. (2010) Geological Map of Slovenia at a scale of 1:250,000.
- Chow, V. Te. (1959) *Open-channel hydraulics*. Blackburn Press. Retrieved from
[https://books.google.com/books/about/Open_channel_Hydraulics.html?id=JAj7sw
EACAAJ](https://books.google.com/books/about/Open_channel_Hydraulics.html?id=JAj7swEACAAJ)
- Clark, K., Ball, J. & Babister, M. (2015) Can Fixed Grid 2D Hydraulic Models Be Used
as Hydrologic Models. *Australian Journal of Water Resources* **19**(1), 74–85.
Taylor and Francis Ltd. doi:10.7158/13241583.2015.11465458
- Coombes, P. J., Colegate, M. & Buchanan, S. (2018) Use of direct rain as an
investigation process and design of basins using ARR2016 methods Use of direct
rain as an investigation process and design of basins using ARR2016 methods
(October).
- Costabile, P., Costanzo, C., Ferraro, D. & Barca, P. (2021) Is HEC-RAS 2D accurate
enough for storm-event hazard assessment? Lessons learnt from a benchmarking
study based on rain-on-grid modelling. *J Hydrol (Amst)* **603**(October).
doi:10.1016/j.jhydrol.2021.126962

- Costabile, P., Costanzo, C., Gandolfi, C., Gangi, F. & Masseroni, D. (2022) Effects of DEM Depression Filling on River Drainage Patterns and Surface Runoff Generated by 2D Rain-on-Grid Scenarios. *Water (Switzerland)* **14**(7). doi:10.3390/w14070997
- Costabile, P., Costanzo, C., Lombardo, M., Shavers, E. & Stanislawski, L. V. (2024) Unravelling spatial heterogeneity of inundation pattern domains for 2D analysis of fluvial landscapes and drainage networks. *J Hydrol (Amst)* **632**. Elsevier B.V. doi:10.1016/j.jhydrol.2024.130728
- David, A. & Schmalz, B. (2021) A systematic analysis of the interaction between rain-on-grid-simulations and spatial resolution in 2d hydrodynamic modeling. *Water (Switzerland)* **13**(17). doi:10.3390/w13172346
- Dimitriadis, P., Tegos, A., Oikonomou, A., Pagana, V., Koukouvinos, A., Mamassis, N., Koutsoyiannis, D., et al. (2016) Comparative evaluation of 1D and quasi-2D hydraulic models based on benchmark and real-world applications for uncertainty assessment in flood mapping. *J Hydrol (Amst)* **534**, 478–492. Elsevier. doi:10.1016/J.JHYDROL.2016.01.020
- Engman, E. T. (1983) Roughness coefficients for routing surface runoff. *Journal of Irrigation and Drainage Engineering-asce*. Am. Soc.Civ. Engrs. doi:10.1061/(ASCE)0733-9437(1986)112:1(39)
- Ficklin, D. L. & Zhang, M. (2013) A Comparison of the Curve Number and Green-Ampt Models in an Agricultural Watershed. *Trans ASABE* **56**(1), 61–69. American Society of Agricultural and Biological Engineers. doi:10.13031/2013.42590
- García-Alén, G., González-Cao, J., Fernández-Nóvoa, D., Gómez-Gesteira, M., Cea, L. & Puertas, J. (2022) Analysis of two sources of variability of basin outflow hydrographs computed with the 2D shallow water model Iber: Digital Terrain

Model and unstructured mesh size. *J Hydrol (Amst)* **612**. Elsevier B.V.

doi:10.1016/j.jhydrol.2022.128182

Gonga-Saholiariliva, N., Gunnell, Y., Petit, C. & Mering, C. (2011) Techniques for quantifying the accuracy of gridded elevation models and for mapping uncertainty in digital terrain analysis. *Prog Phys Geogr* **35**(6), 739–764. SAGE Publications Ltd. doi:10.1177/0309133311409086

Guo, K., Guan, M. & Yu, D. (2021) Urban surface water flood modelling-a comprehensive review of current models and future challenges. *Hydrol Earth Syst Sci* **25**(5), 2843–2860. Copernicus GmbH. doi:10.5194/HESS-25-2843-2021

Gupta, H. V., Kling, H., Yilmaz, K. K. & Martinez, G. F. (2009) Decomposition of the mean squared error and NSE performance criteria: Implications for improving hydrological modelling. *J Hydrol (Amst)* **377**(1–2), 80–91. Elsevier. doi:10.1016/J.JHYDROL.2009.08.003

Habtezion, N., Tahmasebi Nasab, M. & Chu, X. (2016) How does DEM resolution affect microtopographic characteristics, hydrologic connectivity, and modelling of hydrologic processes? *Hydrol Process* **30**(25), 4870–4892. John Wiley and Sons Ltd. doi:10.1002/hyp.10967

Hariri, S., Weill, S., Gustedt, J. & Charpentier, I. (2022) A balanced watershed decomposition method for rain-on-grid simulations in HEC-RAS. *Journal of Hydroinformatics* **24**(2), 315–332. doi:10.2166/hydro.2022.078

Huang, H., Liao, W., Lei, X., Wang, C., Cai, Z. & Wang, H. (2023) An urban DEM reconstruction method based on multisource data fusion for urban pluvial flooding simulation. *J Hydrol (Amst)* **617**, 128825. Elsevier. doi:10.1016/J.JHYDROL.2022.128825

- Khojeh, S., Ataie-Ashtiani, B. & Hosseini, S. M. (2022) Effect of DEM resolution in flood modeling: a case study of Gorganrood River, Northeastern Iran. *Natural Hazards* **112**(3), 2673–2693. Springer Science and Business Media B.V. doi:10.1007/S11069-022-05283-1/METRICS
- Kobold, M. & Sušnik, M. (2001) Hidrološki model Save do Zidanega mosta v programskem okolju WMS. Hidrometeorološki zavod RS. Ljubljana.
- Kobold, M., Sušnik, M., Robič, M., Ulaga, F. & Lalić, B. (2008) Hydrological analysis of high waters and flash floods occurred in September 2007 in Slovenia. *IOP Conf Ser Earth Environ Sci* **4**(December 2008), 012008. doi:10.1088/1755-1307/4/1/012008
- Komac, B. & Zorn, M. (2013) Extreme floods in Slovenia in september 2010. *Springer Geography* (9789400763005), 121–139. Springer. doi:10.1007/978-94-007-6301-2_8/FIGURES/000815
- Krvavica, N., Šiljeg, A., Horvat, B. & Panda, L. (2023) Pluvial Flash Flood Hazard and Risk Mapping in Croatia: Case Study in the Gospić Catchment. *Sustainability* **15**(2), 1197. doi:10.3390/su15021197
- Li, Jing & Wong, D. W. S. (2010) Effects of DEM sources on hydrologic applications. *Comput Environ Urban Syst* **34**(3), 251–261. Pergamon. doi:10.1016/J.COMPENVURBSYS.2009.11.002
- Li, Jun, Wang, Z. & Liu, C. (2015) A combined rainfall infiltration model based on Green-Ampt and SCS-curve number. *Hydrol Process* **29**(11), 2628–2634. John Wiley and Sons Ltd. doi:10.1002/HYP.10379
- Marchi, L., Borga, M., Sangati, M., Preciso, E., Gaume, E., Bain, V., Delrieu, G., et al. (2009) Comprehensive post-event survey of a flash flood in Western Slovenia:

observation strategy and lessons learned. *Hydrol Process* **23**, 3761–3770.

doi:10.1002/hyp

Md Ali, A., Solomatine, D. P. & Baldassarre, G. Di. (2015) Assessing the impact of different sources of topographic data on 1-D hydraulic modelling of floods. *Hydrol Earth Syst Sci* **19**(1), 631–643. Copernicus GmbH. doi:10.5194/HESS-19-631-2015

Muthusamy, M., Casado, M. R., Butler, D. & Leinster, P. (2021) Understanding the effects of Digital Elevation Model resolution in urban fluvial flood modelling. *J Hydrol (Amst)* **596**. Elsevier B.V. doi:10.1016/j.jhydrol.2021.126088

Podhorányi, M., Unucka, J., Bobál', P. & Říhová, V. (2013) Effects of LIDAR DEM resolution in hydrodynamic modelling: model sensitivity for cross-sections. <http://dx.doi.org/10.1080/17538947.2011.596578> **6**(1), 3–27. Taylor & Francis Group . doi:10.1080/17538947.2011.596578

Rusjan, S., Kobold, M. & Mikoš, M. (2009) Characteristics of the extreme rainfall event and consequent flash floods in W Slovenia in September 2007. *Natural Hazards and Earth System Science* **9**(3), 947–956. doi:10.5194/nhess-9-947-2009

Ryan, P., Symen Bill, Gao, S. & Collecutt, G. (2022) Direct Rainfall Hydraulic Model Validation. New South Wales.

Saksena, S. & Merwade, V. (2015) Incorporating the effect of DEM resolution and accuracy for improved flood inundation mapping. *J Hydrol (Amst)* **530**, 180–194. Elsevier. doi:10.1016/J.JHYDROL.2015.09.069

Sebastian, A., Juan, A. & Bedient, P. B. (2022) Urban flood modeling: Perspectives, challenges, and opportunities. *Coastal Flood Risk Reduction: The Netherlands and the U.S. Upper Texas Coast* 47–60. Elsevier. doi:10.1016/B978-0-323-85251-7.00005-6

Su, Y. F., Lin, Y. T., Jang, J. H. & Han, J. Y. (2022) High-Resolution Flood Simulation in Urban Areas Through the Application of Remote Sensing and Crowdsourcing Technologies. *Front Earth Sci (Lausanne)* **9**, 1445. Frontiers Media S.A.

doi:10.3389/FEART.2021.756198/BIBTEX

Union, E. (2018) Imperviousness Density 2006.

Vázquez, R., Carlón-Allende, T., García-Tenorio, F. & Mendiola, F. (2023) Numerical modelling of a flash-flood event at Peribán de Ramos, Michoacán (Mexico).

<https://doi.org/10.1080/02723646.2022.2163539>. Taylor & Francis.

doi:10.1080/02723646.2022.2163539

Viji, R., Prasanna, P. R. & Ilangovan, R. (2015) Modified SCS-CN and Green-Ampt Methods in Surface Runoff Modelling for the Kundahpallam Watershed, Nilgiris, Western Ghats, India. *Aquat Procedia* **4**, 677–684. Elsevier.

doi:10.1016/J.AQPRO.2015.02.087

Vozinaki, A. E. K., Morianou, G. G., Alexakis, D. D. & Tsanis, I. K. (2016) Comparing 1D and combined 1D/2D hydraulic simulations using high-resolution topographic data: a case study of the Koiliaris basin, Greece.

<https://doi.org/10.1080/02626667.2016.1255746> **62**(4), 642–656. Taylor &

Francis. doi:10.1080/02626667.2016.1255746

WMS Manual: Watershed Modeling System. Reference manual. (1997) . Utah.

Xafoulis, N., Kontos, Y., Farsirotou, E., Kotsopoulos, S., Perifanos, K., Alamanis, N.,

Dedousis, D., et al. (2023) Evaluation of Various Resolution DEMs in Flood Risk

Assessment and Practical Rules for Flood Mapping in Data-Scarce Geospatial

Areas: A Case Study in Thessaly, Greece. *Hydrology 2023, Vol. 10, Page 91* **10**(4),

91. Multidisciplinary Digital Publishing Institute.

doi:10.3390/HYDROLOGY10040091

- Xu, K., Fang, J., Fang, Y., Sun, Q., Wu, C. & Liu, M. (2021) The Importance of Digital Elevation Model Selection in Flood Simulation and a Proposed Method to Reduce DEM Errors: A Case Study in Shanghai. *International Journal of Disaster Risk Science* **12**(6), 890–902. Beijing Normal University Press. doi:10.1007/s13753-021-00377-z
- Zanon, F., Borga, M., Zoccatelli, D., Marchi, L., Gaume, E., Bonnifait, L. & Delrieu, G. (2010) Hydrological analysis of a flash flood across a climatic and geologic gradient: The September 18, 2007 event in Western Slovenia. *J Hydrol (Amst)* **394**(1–2), 182–197. Elsevier B.V. doi:10.1016/j.jhydrol.2010.08.020
- Zeiger, S. J. & Hubbart, J. A. (2021) Measuring and modeling event-based environmental flows: An assessment of HEC-RAS 2D rain-on-grid simulations. *J Environ Manage* **285**(July 2020), 112125. Elsevier Ltd. doi:10.1016/j.jenvman.2021.112125
- Zorn, M. & Komac, B. (2011) Damage caused by natural disasters in Slovenia and globally between 1995 and 2010. *Acta Geographica Slovenica* **51**(1), 7–41. ZRC SAZU, Založba ZRC. doi:10.3986/AGS51101

Tables

Table 1: HEC-RAS characteristics of the Selška Sora watershed.

Label	Typology	% of area covered	CN	Manning's n	Abstraction Ratio
1	Discontinuous urban fabric	0.02	98	0.16	0.2
2	Pastures	4.51	75	0.05	0.2
3	Land principally occupied by agriculture, with significant areas of natural vegetation	9.34	86	0.05	0.2
4	Broad leaved forest	19.67	71	0.16	0.1
5	Coniferous forest	28.69	71	0.16	0.1
6	Mixed forest	30.65	71	0.16	0.1
7	Natural grasslands	3.41	60	0.16	0.2
8	Transitional woodland shrub	1.13	54	0.2	0.1
9	Main channel	2.54	64	0.19	0

Table 2: Numerical configuration of the RoG simulation in HEC-RAS

Numerical parameter	Value
Computational interval	1 min
Maximum Courant	1
Minimum Courant	0.45
Number of steps below Minimum before Doubling	10
Maximum number of doubling base time step	1
Maximum number of halving base time step	6

Table 3: RoG simulation results at Železniki station.

KGE	Pearson correlation coefficient	RMSE (m^3s^{-1})
0.913	0.964	22.382

Table 4: Concentration Time per formula or model

Method	Time of Concentration (T_c)
Traditional method 1st peak	1 hour and 45 min
RoG 1st peak	1 hour and 15 min
Traditional method 2nd peak	3 hours
RoG 2nd peak	3 hours and 30 min
Giandotti	3 hours and 54 min
Kirpich	6 hours and 48 min

Table 5: Coefficient of Variation (CV) per DEM resolution

DEM resolution	1 m	5 m	10 m	15 m	20 m	25 m	30 m
CV	29.65	29.60	29.60	29.61	29.53	29.65	29.65

Table 6: Performance metrics of hydraulic simulation per resolution.

Resolution	KGE	Pearson correlation coefficient	RMSE (m^3s^{-1})
1 m	0.913	0.964	22.382
5 m	0.878	0.915	33.269
10 m	0.873	0.914	33.626
15 m	0.803	0.911	34.764
20 m	0.816	0.906	35.429
25 m	0.577	0.908	43.316
30 m	0.713	0.904	38.150

Table 7: First and second peak discharge values (m^3s^{-1}).

	Benchmark	1 m	5 m	10 m	15 m	20 m	25 m	30 m
First peak (m^3s^{-1})	277	284	278	275	258	263	213	240
Second peak (m^3s^{-1})	120	139	169	170	155	160	126	138

Table 8: Courant raster statistics

	DEM 1 m resolution	DEM 30 m resolution
Minimum	10^{-7}	10^{-5}
Mean	0.22	0.36
Maximum	5.82	7.63
Standard Deviation	0.47	0.50

Table 9: Velocity raster statistics (ms⁻¹)

	DEM 1 m resolution	DEM 30 m resolution
Minimum	10 ⁻⁴	10 ⁻³
Mean	1.53	1.38
Maximum	15.28	10.19
Standard Deviation	0.47	0.50

Figure captions

Figure 1: Elevation of the watershed, displaying the ARSO rainfall (blue) station and discharge station at the outlet (black)

Figure 2: Land cover classification in the watershed. The classification refers to the Typology depicted in Table 1.

Figure 3: Precipitation (mm), along with ARSO and RoG discharge (m^3s^{-1}).

Figure 4: ARSO flood extent and simulated water depth at Železniki station.

Figure 5: Elevation curves within the overestimated simulation depth.

Figure 6: Time series for the observed and simulated (RoG) discharge for 17/09/2010.

Figure 7: Main statistics post-DEM resampling.

Figure 8: Main statistics post-DEM resampling – slope values.

Figure 9: Elevation relative frequency distribution at the 1 and 30 m resolution (%).

Figure 10: Variation of DEM resolution vs. model performance.

Figure 11: DEM ensemble hydrograph at the Železniki station (m^3s^{-1}).

Figure 12: Boxplot representing distribution of depth-difference rasters. Negative values reflect greater depth as the resolution is coarsened. Greater spread observed between different resolutions corresponds to greater depth-difference variability across the domain.

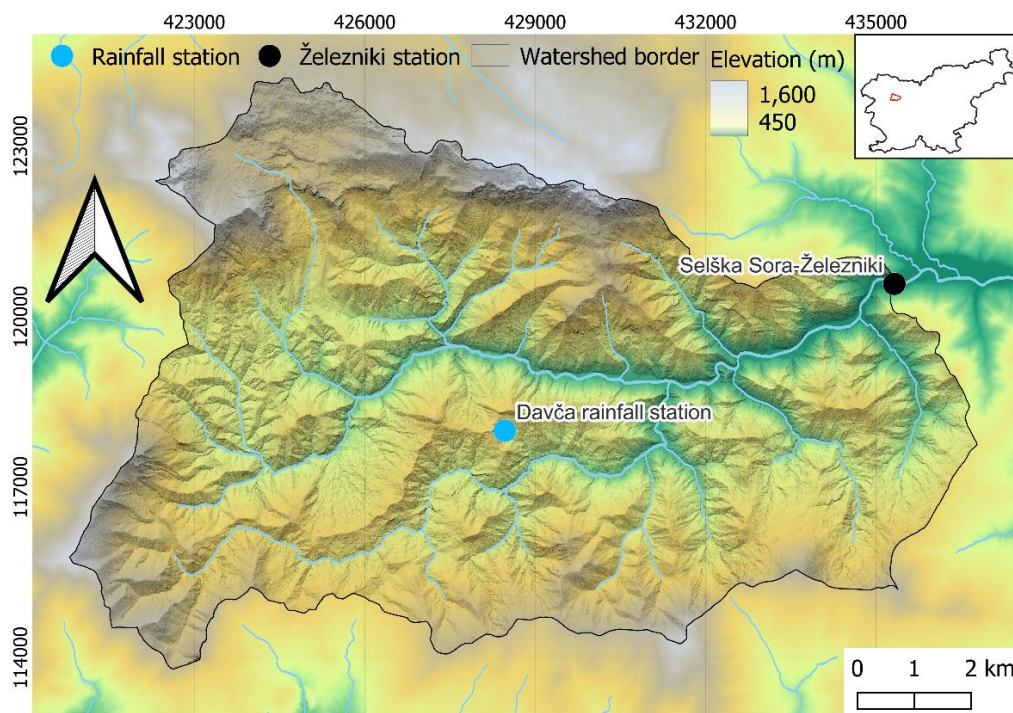
Figure 13: Time series of computation time and KGE performance across DEM resolutions.

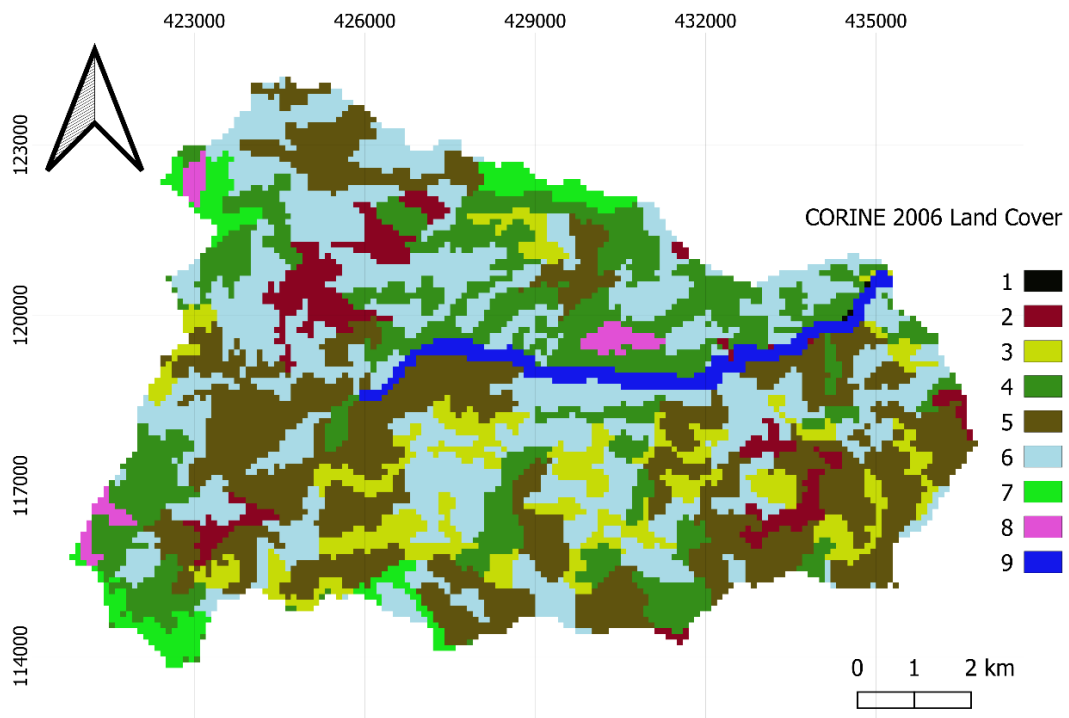
Figure 14: Rating curve (a) and volume accumulation (b) between 1 and 30 m DEM resolution.

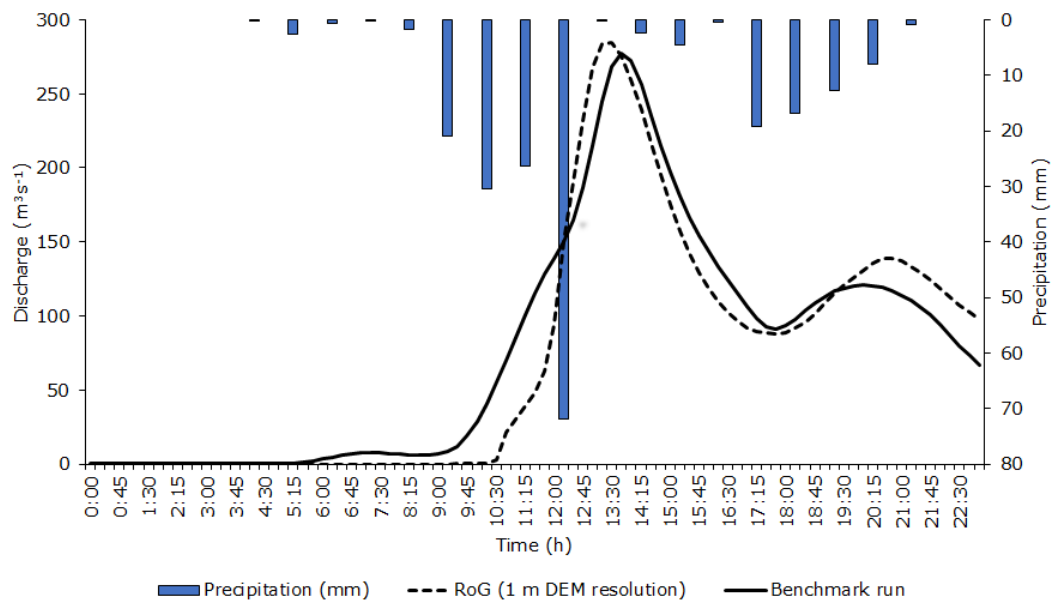
Figure 15: Courant number at the channel for 1 and 30 m DEM resolution – timestamp: 12:15 PM.

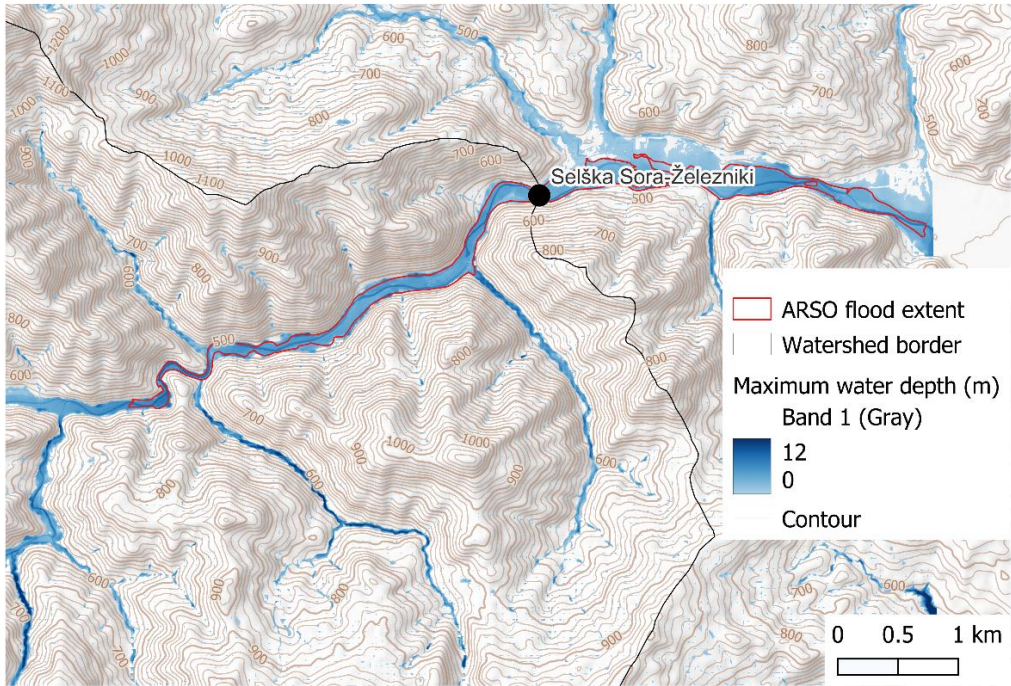
Figure 16: Velocity (max) ms^{-1} for the 1 m and 30 m DEM resolution.

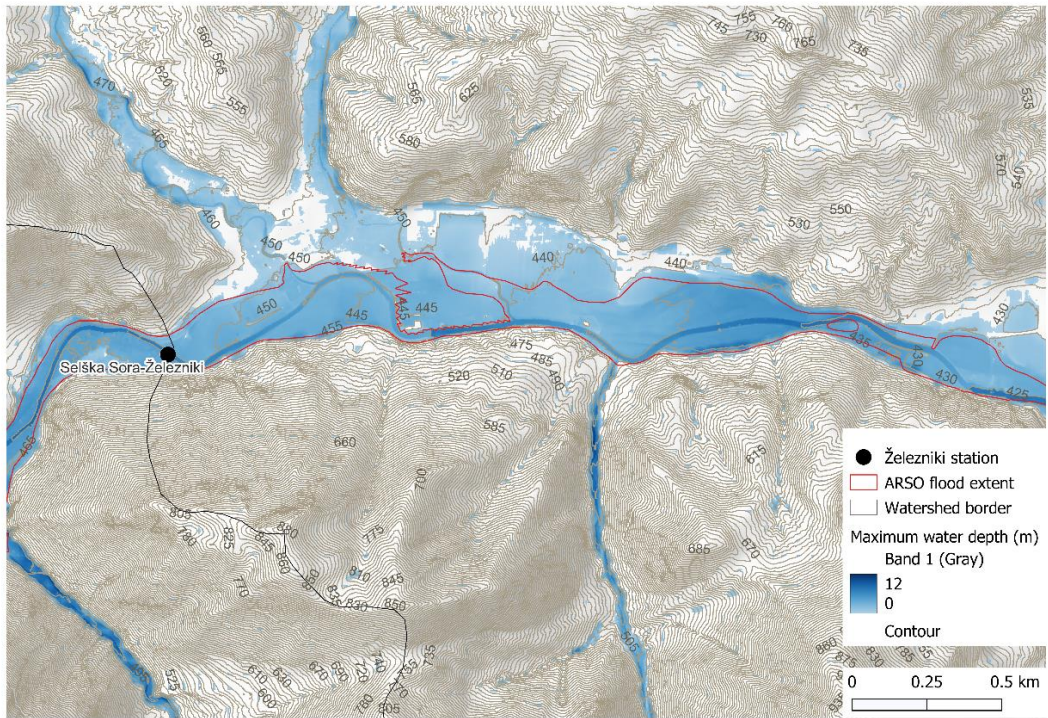
Figures

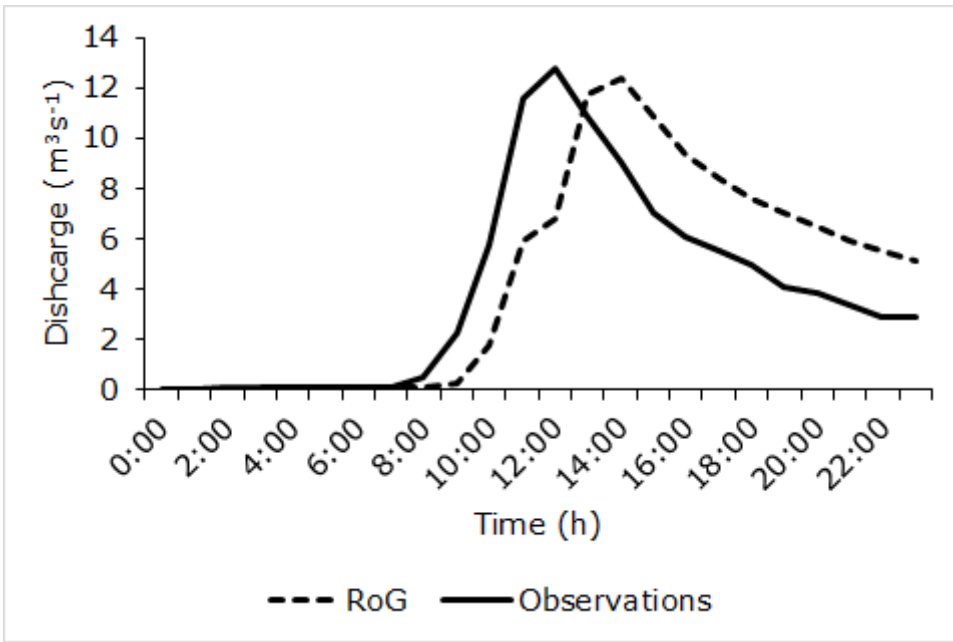


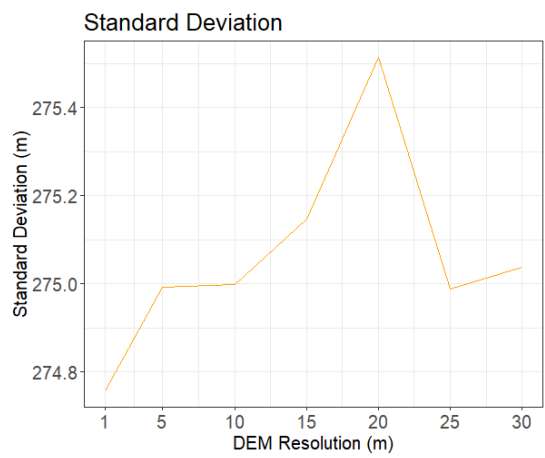
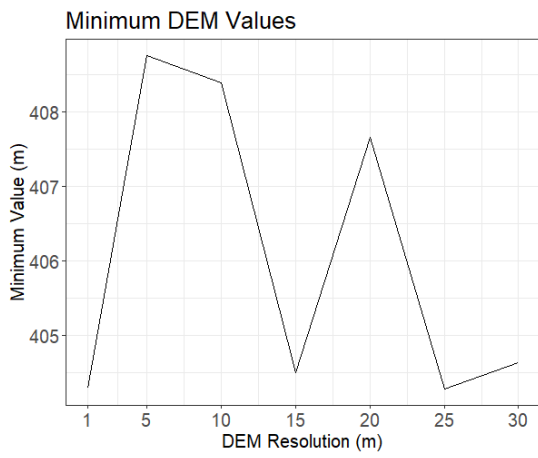
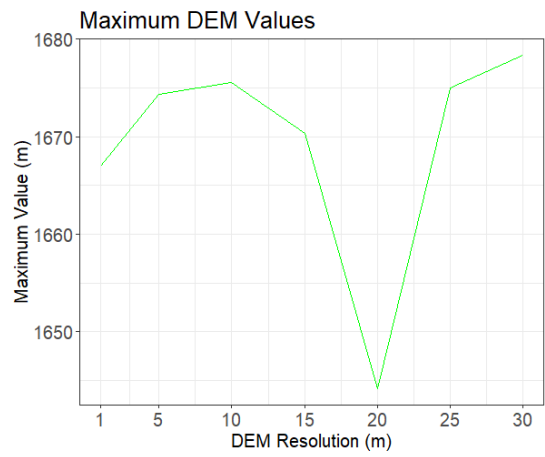
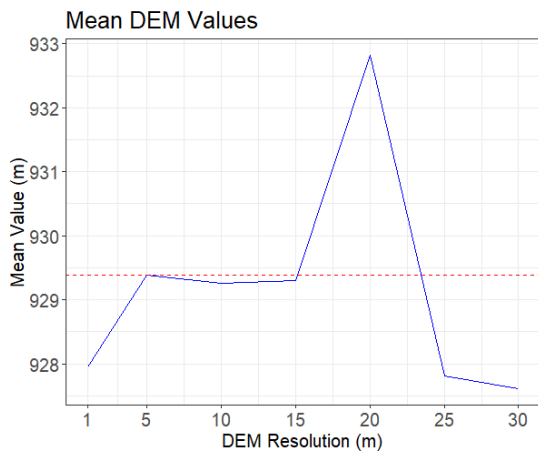




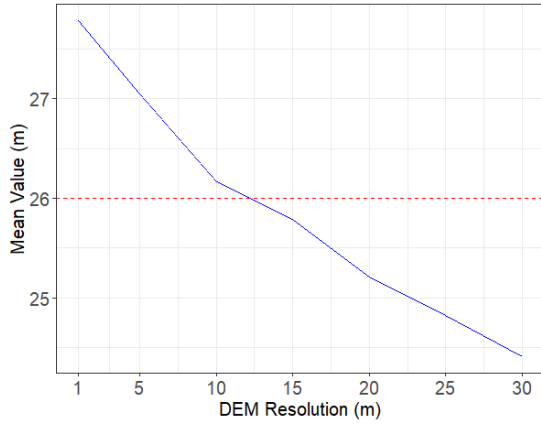




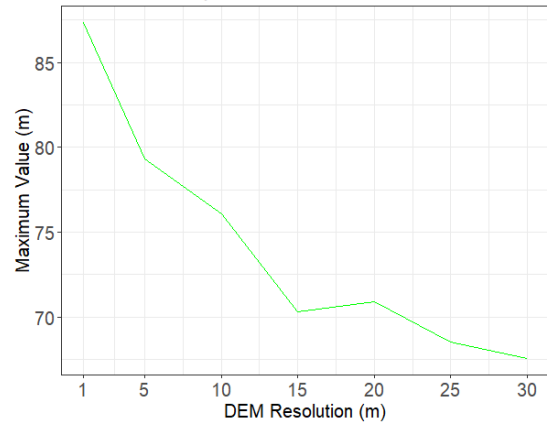




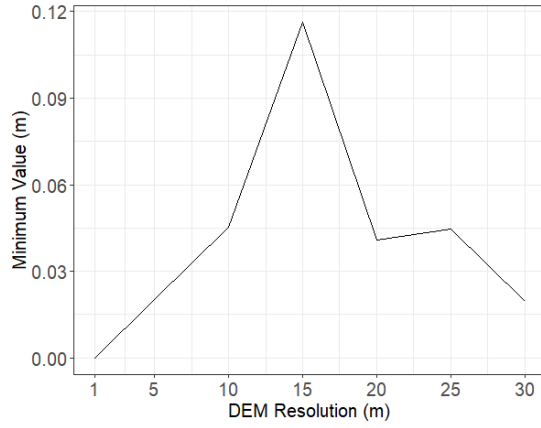
Mean Slope Values



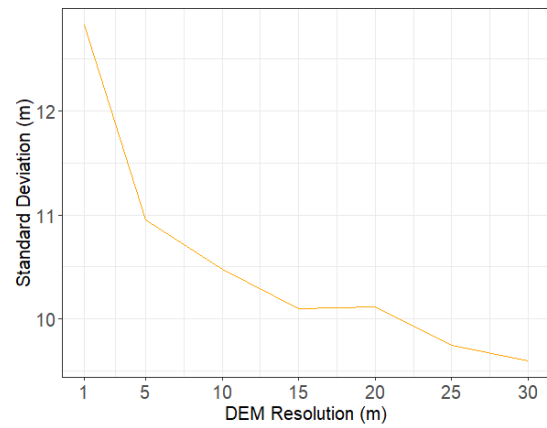
Maximum Slope Values



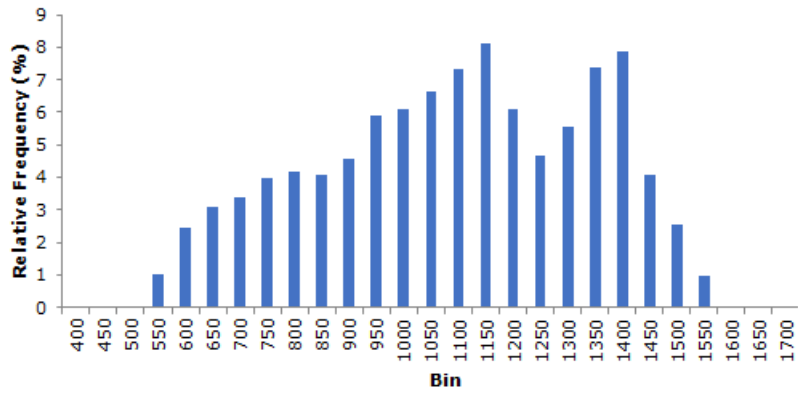
Minimum Slope Values



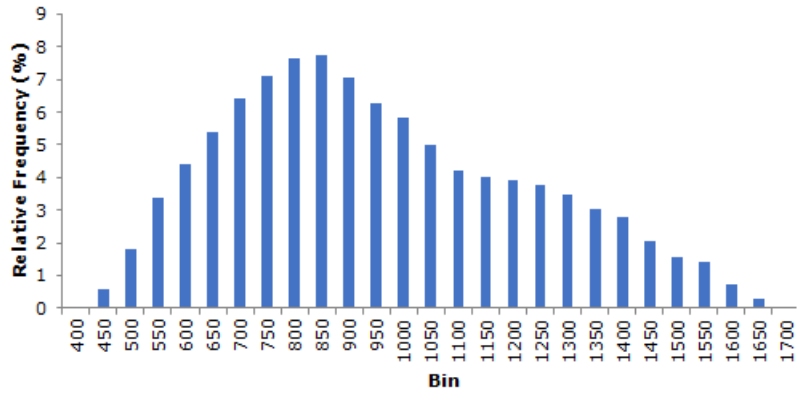
Standard Deviation

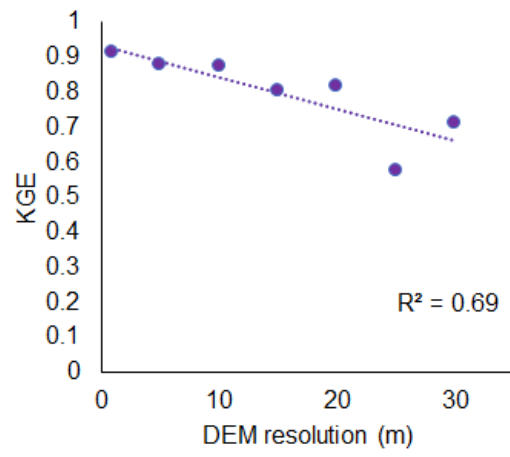
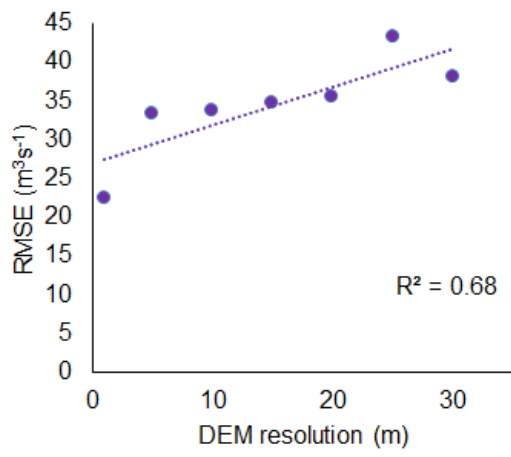


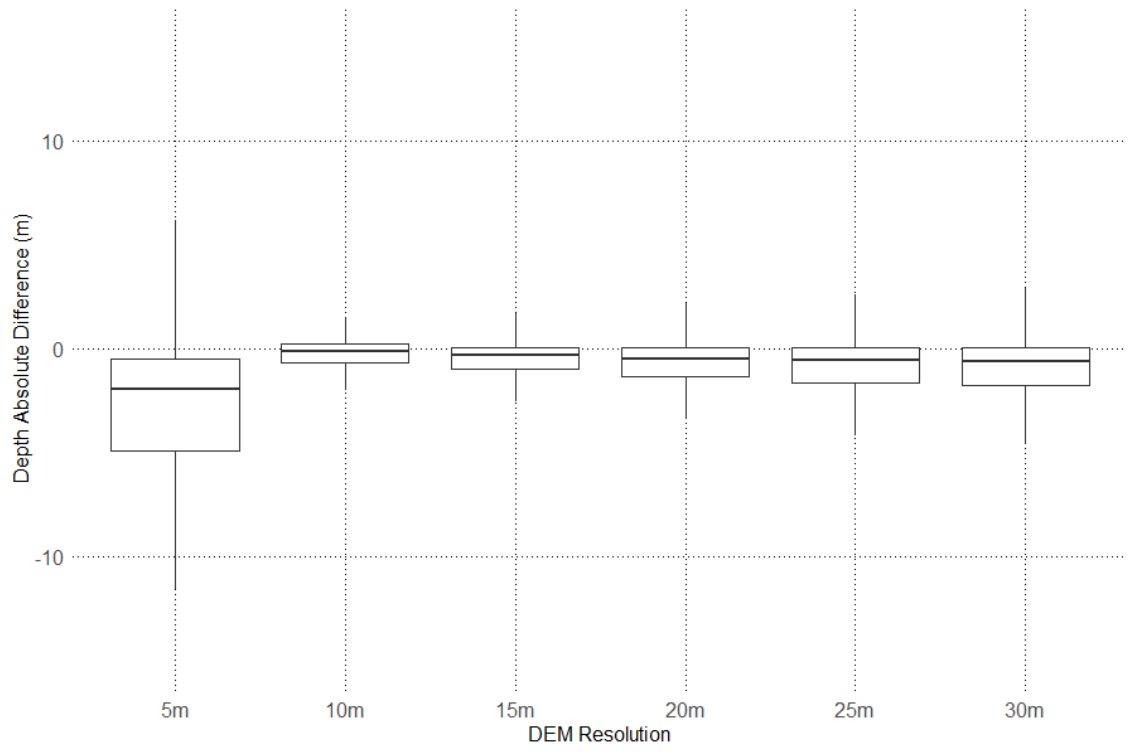
DEM - 1 m resolution

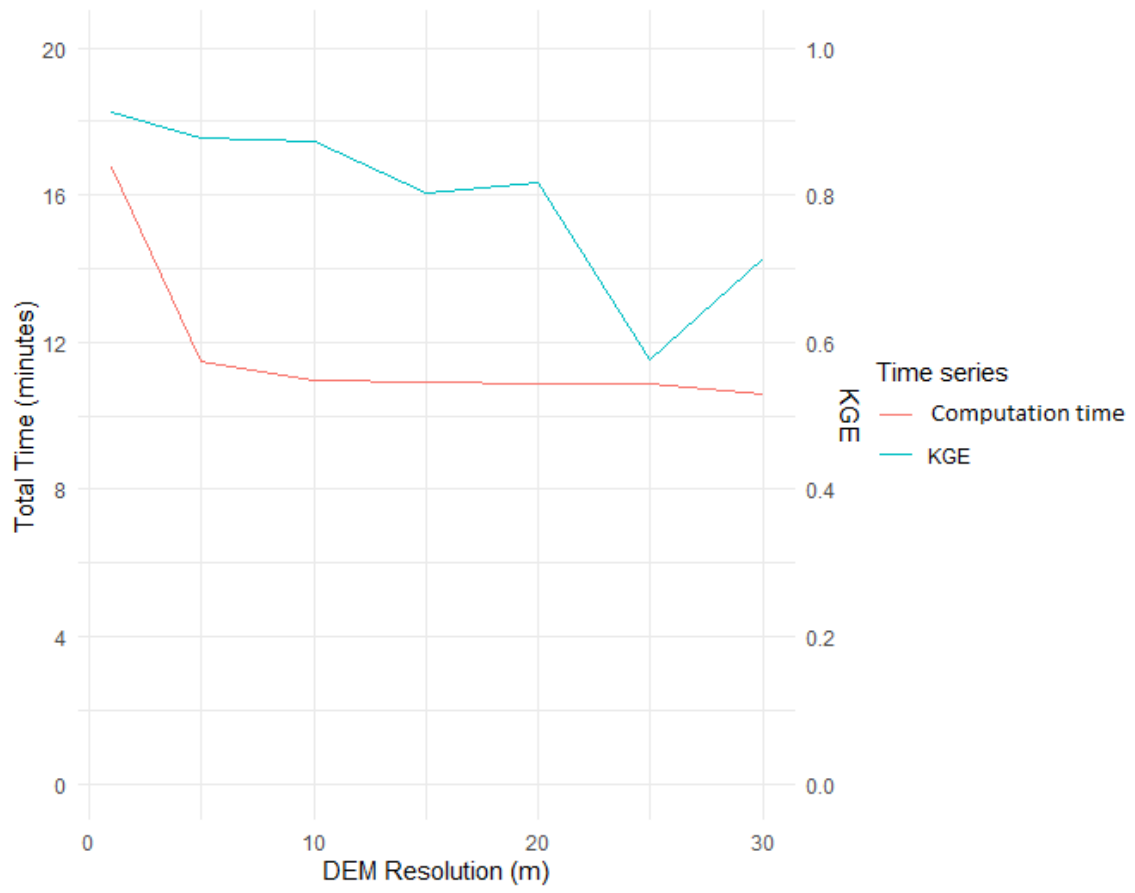


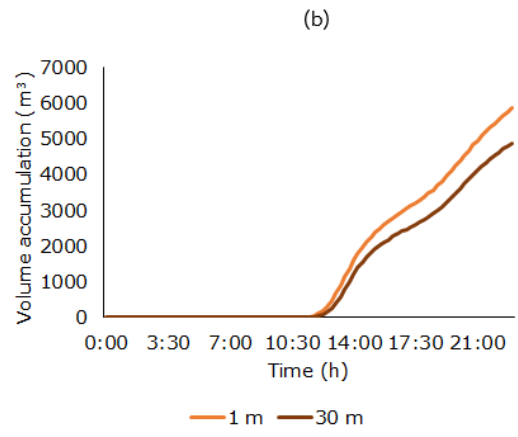
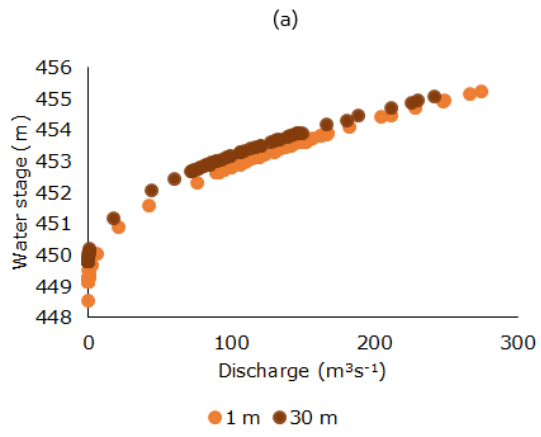
DEM - 30 m resolution

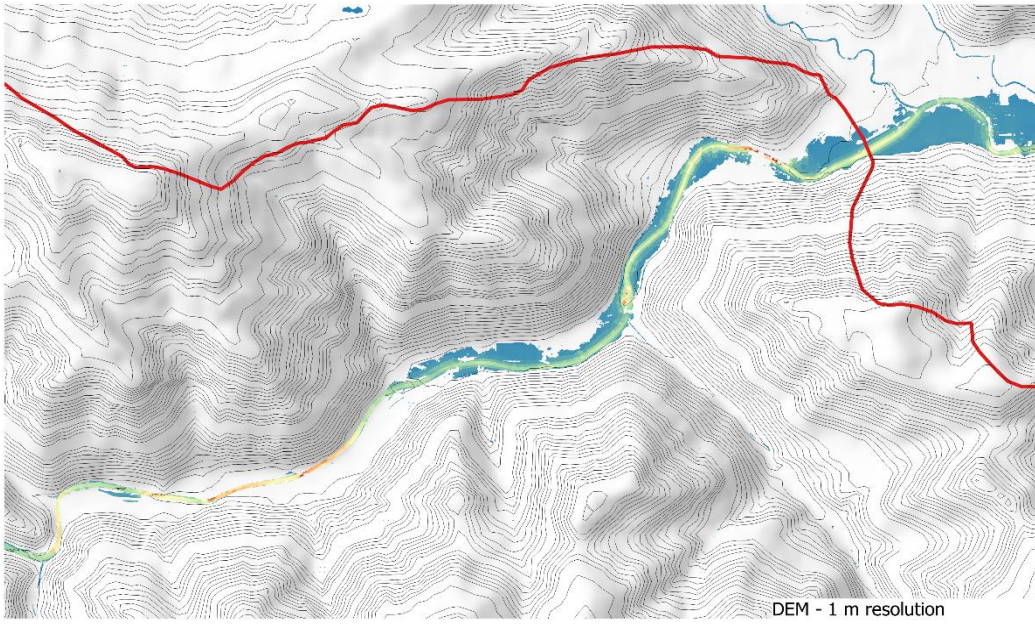












Courant number Range 2 0

Watershed border

Contour lines

Time frame: 12:15 PM
18/09/2007

